

Climate dynamics and time series analysis of ice-core records.

Peter D. Ditlevsen

The Niels Bohr Institute, Department for Geophysics,
University of Copenhagen, Juliane Maries Vej 30,
DK-2100 Copenhagen O, Denmark.

June 3, 2002

The climate on the Earth varies on many different spatial and temporal scales. In order to understand the predictability and dynamical origin of climatic changes we need very long records. The instrumental records of temperatures and other meteorological parameters only date about a century back. This is too short a period to obtain the full range of natural variability, which is the background on which eventual man caused climate changes must be assessed. Climate variations dating much further back, most prominent being the big ice-ages, are recorded through geological markings, such as the characteristic moraine landscapes created by the glaciers. Other more detailed paleoclimatic records are tree-ring thickness, corals, lake and ocean sediments and ice-core records. All of these indicators are indirect recordings, which are more or less local in nature, of the past climate. Some of the longest records with high temporal resolution are the ice-core records. From analysis of these records it is possible to deduce part of the dynamical behavior of the climate system. Before performing an analysis of the ice-core series a few basic tools applied in climate data analysis will be derived and reviewed, in order to make this text self-contained for readers not familiar with all the details in statistical analysis of time series.

Contents

Basic time series analysis	3
A few types of signals	5
Stochastic climate models	7
The Fokker-Planck equation	10
The potential and the stationary distribution	12
Stochastic resonance	15
Ice-core records	16
Separating time scales	17
The Dansgaard/Oeschger events	18
The climatic noise and intermittency	20
Exotic statistics	21
Summary and outlook	23
References	25

Basic time series analysis

When investigating a climatological time series one would be interested in characterizing and quantifying to what degree the signal is periodic, persistent, random, chaotic etc. Figure 1 shows three examples of present days direct climatic time series. Figure 1 (a) shows the twice daily (12 noon and 12 midnight) temperatures in Nuuk, Greenland through two years (1985-86). Figure 1 (b) shows the annual mean global temperature anomaly, which is the estimated area averaged global temperature with the 1951-80 mean subtracted. Finally, figure 1 (c) shows the Southern Oscillation Index (SOI) which is the sea surface pressure difference between Tahiti and Darwin (Australia). This index is related to the El Nino in the Pacific. The three time series seems quite different. The first contains a strong periodic component, the annual cycle. The second seems to vary with a trend all the way through the record, while the third seems to vary irregularly with a typical time scale of 3-6 years. Imagine that the series were all we had to predict the future development of the curves. In the first case we have some idea that a few days ahead the temperature will be about the same, 6 months ahead the season will have changed so if its summer now it will be colder in 6 months and visa versa. In the second case we can see that the variations over, say, a decade is relatively small so that if we have a cold/warm anomaly the same will probably be true in 10 years, but not in 30 years. On top of that there seems to be an overall positive trend. In the third case the signal seems to have forgotten its value after about 1-2 years which would then be the prediction limit, if we could only predict from the signal itself.

This kind of memory in the signal is characterized in the autocorrelation function which is defined as,

$$c(\tau) = \langle x(t)x(t+\tau) \rangle \equiv \lim_{T \rightarrow \infty} \frac{1}{T} \int_{-T/2}^{T/2} x(t)x(t+\tau)dt. \quad (1)$$

It follows directly from the definition that $c(-\tau) = c(\tau)$ and $c(0) > 0$ is the variance of x plus the mean of x squared, which we can always take to be zero by defining x as the deviation from the mean (the anomaly) as has been done in figures 1 (b),(c). The autocorrelation function indicates how quickly the signal varies. The autocorrelations corresponding to figure 1 are shown in figure 2.

The autocorrelation of a pure harmonic signal, $x(t) = x_0 \cos(\omega t)$, is easily calculated. Since the signal is periodic it is enough to integrate over one

period, and we get,

$$c(\tau) = \frac{x_0^2}{2\pi/\omega} \int_{-\pi/\omega}^{\pi/\omega} \cos(\omega t) \cos(\omega(t + \tau)) dt = \frac{x_0^2}{2} \cos(\omega\tau). \quad (2)$$

Compare this with figure 2 (a), here there is a small oscillation on top of a smooth curve. This oscillation reflects the diurnal cycle with warmer temperatures at noon and colder temperatures at midnight. Figure 2 shows that for τ larger than some characteristic time T the autocorrelation becomes numerically small in comparison to the variance $c(0)$. This time T , which will be defined more precisely later, is called the correlation time. It is the typical time scale for the memory in the system.

An equivalent way of describing a signal is by calculating the spectral density or power spectrum of the signal. This is defined from the Fourier transformed, $\hat{x}(\omega) = \lim_{T \rightarrow \infty} \int_{-T/2}^{T/2} x(t) \exp(i\omega t) dt$, of the signal as,

$$P(\omega) = \hat{x}(\omega) \hat{x}(-\omega). \quad (3)$$

The power spectrum is, as the autocorrelation function, symmetric so that we always only consider $\omega > 0$ (and $\tau > 0$ for the autocorrelation function). Furthermore, since the signal is real we have $\hat{x}(-\omega) = \hat{x}(\omega)^*$ and the power spectrum is positive. The power spectrum tells how much weight the signal has on each frequency but nothing about the phases of the wave-components at that frequency. The power spectrum is simply the Fourier transformed of the autocorrelation function:

$$\begin{aligned} \hat{c}(\omega) &= \int c(\tau) \exp(i\omega\tau) d\tau = & (4) \\ & \int \int x(t) x(t + \tau) \exp(i\omega(t + \tau)) \exp(-i\omega t) dt d\tau = \\ & \int \left\{ \int x(t + \tau) \exp(i\omega(t + \tau)) d(t + \tau) \right\} x(t) \exp(-i\omega t) dt = \\ & \hat{x}(\omega) \hat{x}(-\omega) = P(\omega). \end{aligned}$$

Here we have suppressed integration boundaries (remember that we define $\int = \int_{-\infty}^{\infty} = \lim_{T \rightarrow \infty} \int_{-T/2}^{T/2}$), interchanged integrations, and translated one integration variable. It is left to the reader to show that the symmetry of the autocorrelation function ensures the positivity of the power spectrum. From this it follows that the Fourier transforms can be expressed as

$$P(\omega) = 2 \int_0^{\infty} c(t) \cos(\omega t) dt, \quad (5)$$

$$c(t) = 2 \int_0^{\infty} P(\omega) \cos(\omega t) d\omega. \quad (6)$$

The power spectra of the signals in figure 1 are shown in figure 3. Figure 3 (a) shows that there is a periodic component of the signal in figure 1 (a), with a period of 1 year.

A given climate signal will in general be composed of variations from many different causes and on many different time scales. This means that the signal will have spectral weight on many frequencies. When analyzing such a signal, in order to understand the dynamics governing the signal, it is often helpful to characterize it in terms of a few simple types of power spectra.

A few types of signals

Periodic signals

Periodicities such as the diurnal and annual cycles will naturally occur in climate signals. Other oscillatory external forcings, such as the 11 years Sun spot cycle or the orbital Milankovitch cycles, can also be identified in climate variations. Finally, the possibility of internal dynamical oscillations or limit cycles in climate dynamics are of interest. The autocorrelation function for the harmonic signal, $x = x_0 \cos(\omega_0 t)$ was found in (2). From this the power spectrum is easily calculated using Eulers formula,

$$\begin{aligned} P(\omega) &= \int \frac{x_0^2}{2} \cos(\omega_0 t) \exp(i\omega t) dt = & (7) \\ \frac{x_0^2}{4} \int (\exp(i(\omega + \omega_0)t) + \exp(i(\omega - \omega_0)t)) dt &= \\ \frac{x_0^2}{2} (\delta(\omega + \omega_0) + \delta(\omega - \omega_0)), & \end{aligned}$$

where the δ -function (which is really a distribution) is defined by:

$$\delta(x) = 0 \text{ for } x \neq 0 \quad (8)$$

$$\int \delta(x) f(x) dx = f(0). \quad (9)$$

So for the integral of the power spectrum we have, taking $\omega_0 > 0$,

$$c(0) = 2 \int_0^\infty P(\omega) d\omega = 2 \int_0^\infty \frac{x_0^2}{2} \delta(\omega - \omega_0) d\omega = x_0^2. \quad (10)$$

So the integral of the power spectrum is another way of expressing the variance of the signal. A periodic signal with period τ can be expressed as a Fourier series,

$$x(t) = \sum_{n=-\infty}^{\infty} c_n \exp(i2\pi n(t/\tau)). \quad (11)$$

It is left as an exercise to find the power spectrum of this signal. Consider what this is in terms of overtones.

Random signals

As we will discuss shortly, a natural way of describing the chaotic and erratic part of the variations is to consider the signal to be random. The most commonly used model of a random signal is that of an independent identically distributed (i.i.d) signal (with zero mean). Such a signal is generated by picking at each sampling time a random (stochastic) variable from a given distribution, independently from any previously chosen variable. For $\tau \neq 0$ the autocorrelation for this signal must vanish since each data point is independent from the other points, $\langle x(t)x(t+\tau) \rangle = \langle x(t) \rangle \langle x(t+\tau) \rangle = 0$. For $\tau = 0$ the autocorrelation just gives the variance, $\langle x^2 \rangle = \sigma^2$, of the signal. Thus we have

$$c(t) = \sigma^2 \delta(t). \quad (12)$$

The power spectrum is then,

$$p(\omega) = \int c(t) \exp(i\omega t) dt = \sigma^2 \int \delta(t) \exp(i\omega t) dt = \sigma^2. \quad (13)$$

This signal has equal weight on all frequencies and is therefore, in analogy to the spectrum of visible light, called white noise. Other continuous spectra with weight on low/high frequencies are, from the same analogy, termed red/blue noise.

Scaling noise

In many chaotic dynamical systems the power spectrum of the variables has a power-function power spectrum,

$$P(\omega) \sim \omega^\alpha. \quad (14)$$

This relationship turns up as straight lines with slope α on log-log plots, which are therefore often used when plotting power spectra. The power-function relation is also called a scaling relation since we have $P(\lambda\omega) = \lambda^\alpha P(\omega)$. An important consequence is that within the range of frequencies or time scales fulfilling the scaling relation there are no characteristic time scales. The generic physical examples are turbulence, where the flow in the inertial range has a self-similar structure, and critical phenomena where at the critical point the spatial correlation structure also shows self-similarity, describable in terms of renormalization group theory. Understanding to which extent these two examples are relevant for describing climate is one of the fundamental challenges in climate research. The white noise is a scaling noise signal, other power-function spectra can sometimes be predicted from scaling properties of the governing dynamical equations or be seen in the data from the behavior of a range of quite complex systems. They are also frequently seen in climatic data. When $\alpha \approx -1$ this is called $1/f$ (one over f) noise, which is seen in a wide range of phenomena.

Stochastic climate models

The climate is characterized by the interaction between components with very different typical time scales. The atmospheric variations, weather patterns, are typically of days to weeks duration while variations in ocean currents are on much longer time scales, years to centuries. The forcing of the slowly varying components, ocean, ice-sheets, comes from the atmosphere through wind, heat exchange, precipitation etc. So the time scales where the slow climate variables change appreciably are beyond the correlation time for the fast variables. At these time scales the fast variables are effectively decorrelated and could then be described as stochastic [21]. Assume that we can describe the system by a set of governing equations for the system variables which can be split in separate variables represented by the vectors $x = (x_1, \dots, x_i, \dots)$ and $y = (y_1, \dots, y_j, \dots)$,

$$\begin{aligned}\dot{x} &= f(x, y) \\ \dot{y} &= g(x, y)\end{aligned}\tag{15}$$

where we can associate a typical time scale τ_{x_i} and τ_{y_j} respectively to each variable such that $\tau_{x_i} \ll \tau_{y_j}$ for all i, j . The second equation describes the dynamics of the large scale observable. For brevity we drop vector notations, and consider x and y as scalar variables. The extension to more dimensions is mostly straight forward. In the effective dynamics for y we can write the small scale variable as $x = \langle x|y \rangle + x'$, where the bracket denotes the average of x conditioned on y . Inserting this into the second equation, using that x varies much faster than y we obtain,

$$\dot{y} = g(\langle x|y \rangle + x', y) \approx g(\langle x|y \rangle, y) + \partial_x g(\langle x|y \rangle, y)x' = g_{\text{eff}}(y) + \sigma(y)\eta.\tag{16}$$

Here we have substituted a stochastic white noise, $\eta(t)$, with $\langle \eta(t)\eta(t') \rangle = \delta(t - t')$ for the short time correlated variations $x'(t)$. The noise intensity is $\sigma(y) = \partial_x g(\langle x|y \rangle, y)\sqrt{\langle x'^2 \rangle}$. The last term will depend on the first equation in (15). The equation (16) is called a Langevin equation. In the simplest form we will assume the noise intensity to be independent of the climate state y , rewriting $F(y) = g_{\text{eff}}(y)$ we have,

$$\dot{y} = F(y) + \sigma\eta.\tag{17}$$

If the noise is small the y component will in one dimension settle into a stable fixed point, y_0 , defined by $F(y_0) = 0$ and $F'(y_0) \equiv -\alpha < 0$. Without loss of generality we can take $y_0 = 0$ and expand $F(y)$ in (17) to first order,

$$\dot{y} = -\alpha y + \sigma\eta.\tag{18}$$

This is called the Ornstein-Uhlenbeck process [16]. A simulation of this stochastic differential equation for y is shown in figure 5. The equation (18) for y can be used to derive a linear differential equation for the autocorrelation function for y :

$$\frac{d}{d\tau}c_y(\tau) = \frac{d}{d\tau} \int y(t)y(t + \tau)dt =\tag{19}$$

$$\begin{aligned}
\int y(t)\dot{y}(t+\tau)dt &= \int y(t)(-\alpha y(t+\tau) + \sigma\eta(t+\tau))dt = \\
&= -\alpha \int y(t)y(t+\tau)dt + \sigma \int y(t)\eta(t+\tau)dt = \\
&= -\alpha c_y(\tau).
\end{aligned}$$

The integral involving $y(t)$ and $\eta(t+\tau)$ vanishes for $\tau > 0$ since η is an independent (white) noise. From this it follows that $c_y(\tau) = c_0 \exp(-\alpha\tau)$ for $\tau > 0$. It is left to the reader to show that $c_y(\tau) = c_0 \exp(\alpha\tau)$ for $\tau < 0$. The solution to (20) is,

$$c_y(\tau) = c_0 \exp(-\alpha|\tau|). \quad (20)$$

The prefactor $c_0 = c_y(0) = \langle y^2 \rangle$ is the variance of the process y which will be determined using the fluctuation-dissipation theorem shortly. The system has a typical time scale of memory, α^{-1} , which is the time it takes for the autocorrelation to drop by a factor of e . It is solely determined by the dynamics of y (through $F(y)$). The power spectrum of y is the Fourier transformed of the autocorrelation function given in (20):

$$\begin{aligned}
P_y(\omega) &= \int c_0 \exp(-\alpha|t|) \exp(i\omega t) dt = \\
c_0 \int_0^\infty \{ \exp((- \alpha + i\omega)t) + \exp((- \alpha - i\omega)t) \} dt &= \\
c_0 \left(\frac{1}{\alpha + i\omega} + \frac{1}{\alpha - i\omega} \right) &= c_0 \frac{2\alpha}{\omega^2 + \alpha^2}.
\end{aligned} \quad (21)$$

The autocorrelation function and the power spectrum are shown in figure 4. For $\omega \ll \alpha$ we have $P(\omega) \sim 1$, that is, y itself is a white noise signal on time scales long in comparison to the typical time scales of the y -dynamics. For $\omega \gg \alpha$ we have $P(\omega) \sim \omega^{-2}$, which is a scaling red noise spectrum.

In general η need not be a white noise. We can derive a relation between the autocorrelation functions of y and η from (18). Starting with the autocorrelation function for η , $c_\eta(\tau)$, using (18) to express η in terms of y and integrating by parts we get,

$$\begin{aligned}
\sigma^2 c_\eta(\tau) &= \sigma^2 \int \eta(t)\eta(t+\tau)dt = \\
&= \int (\dot{y}(t) + \alpha y(t))(\dot{y}(t+\tau) + \alpha y(t+\tau))dt =
\end{aligned} \quad (22)$$

$$\begin{aligned} & \frac{d}{d\tau} \int \dot{y}(t)y(t+\tau)dt + \alpha^2 \int y(t)y(t+\tau)dt + \\ & \alpha \int \{\dot{y}(t)y(t+\tau) + y(t)\dot{y}(t+\tau)\}dt = \\ & \left(-\frac{d^2}{d\tau^2} + \alpha^2\right)c_y(\tau) \end{aligned}$$

where the boundary terms in $\pm\infty$ vanish. From this it follows that the integration constant c_0 can be determined from the variance, σ^2 . By Fourier transforming the autocorrelation functions for η and y we immediately get the expression,

$$P_y(\omega) = \frac{P_\eta(\omega)}{\omega^2 + \alpha^2}. \quad (23)$$

If η is a white noise source, we get the result from before,

$$P_\eta(\omega) \sim 1 \Rightarrow P_y(\omega) \sim \frac{1}{\omega^2 + \alpha^2}. \quad (24)$$

The Fokker-Planck equation

The Langevin equation (16) results in a stochastic realization, $y(t)$, of the signal depending on the specific history of the noise. However, a deterministic behavior is recovered for the probability density. The probability density will fulfil a diffusion equation, the Fokker-Planck equation, which expresses the probability density for the variable y as a function of time, given some known initial condition. Because of the central role played by diffusion in a large class of physical problems, we will give a short heuristic derivation of the Fokker-Planck equation from the Langevin equation. For doing that, we rewrite the Langevin equation in mathematics jargon,

$$dx = f(x)dt + \sigma(x)dB. \quad (25)$$

Here dx denotes the increment in x during time dt under the influence of a drift $f(x)dt$ and a diffusion σdB . The noise dB is called a Brownian motion and it will be clear shortly why this is called a diffusion.

Brownian motion and coin tossing

The Brownian motion is the continuum limit of a sum of independent stochastic increments with a finite variance. Due to the central limit theorem, this

will always result in a gaussian distribution independent of the distribution for the individual increments. We can thus construct the Brownian motion from a sum of coin tosses, or a discrete random walk. The increment ΔB over the time interval Δt is defined as a sum of N coin tosses with values $X_i = \pm 1 \times \sigma(N)$. The mean and variances are simply $\langle X_i \rangle = 0$ and $\langle X_i^2 \rangle = \sigma(N)^2$. We thus have,

$$\Delta B = \sum_{i=1}^N X_i, \quad (26)$$

from which we have $\langle \Delta B \rangle = 0$ and $\langle \Delta B^2 \rangle = N\sigma(N)^2$. Since we want to perform the limit $N \rightarrow \infty$ this must be independent of N and we get $\sigma(N) = C(\Delta t)/\sqrt{N}$. Now by doing the same calculation on the time interval $m\Delta t$ we obtain the equation $m[C(\Delta t)]^2 = [C(m\Delta t)]^2$ with the solution $C(\Delta t) = \sqrt{\Delta t}$. Finally, in the continuum limit we obtain the statistics for the Brownian increment,

$$\langle dB \rangle = 0, \langle dB^2 \rangle = dt \quad (27)$$

This is the fundamental ingredient for deriving the Fokker-Planck equation and the starting point for the Itô calculus which we shall not describe here.

The conditional probability

The Fokker-Planck equation describes the development of the conditional probability $p(x, t|x_0, t_0)$. The conditional probability is just the probability density for the value x at time t given that the system was in state x_0 at time t_0 . The conditional probability will fulfil the obvious relation, called the Chapman-Kolmogorov equation,

$$p(x, t|x_0, t_0) = \int dy p(x, t|y, t_1)p(y, t_1|x_0, t_0), \quad t_0 < t_1 < t \quad (28)$$

which just sums all the possible paths between $x_0(t_0)$ and $x(t)$ at time t_1 . The Fokker-Planck equation can be derived as a differential form of this equation. The Fokker-Planck equation is a partial differential for the conditional probability. Here we will derive it in a straight forward way by introducing an arbitrary stochastic function $\psi[x(t)]$ of the position $x(t)$. The value of the function at time $t + dt$ can be expressed through a Taylor expansion,

$$\psi[x + dx] = \psi[x] + \psi'[x]dx + \psi''[x]dx^2/2 + o(dx^3). \quad (29)$$

We can now perform an average with respect to the increments (25),

$$\langle dx \rangle = f(x)dt, \quad \langle dx^2 \rangle = \sigma^2(x)\langle dB^2 \rangle + o(dt^2) = \sigma^2 dt + o(dt^2), \quad (30)$$

and we obtain the following to first order in dt ,

$$d\psi[x] = \psi[x + dx] - \psi[x] = \{\psi'[x]f(x) + \psi''[x]\sigma^2(x)/2\}dt. \quad (31)$$

This is Itô's formula for the derivative of a stochastic function. To derive the equation for the conditional probability we express the derivative of the mean of the stochastic function conditioned on the position $x_0(t_0)$,

$$\frac{d}{dt}\langle \psi[x] \rangle = \frac{d}{dt} \int dx \psi[x] p(x, t|x_0, t_0) = \int dx \psi[x] \partial_t p(x, t|x_0, t_0) \quad (32)$$

This can as well be expressed using (31) as,

$$\begin{aligned} \frac{d}{dt}\langle \psi[x] \rangle &= \frac{\langle d\psi[x] \rangle}{dt} = \left\langle \partial_x(\psi[x])f(x) + \partial_x^2(\psi[x])\frac{\sigma^2(x)}{2} \right\rangle \\ &= \int dx \left\{ \partial_x(\psi[x])f(x) + \partial_x^2(\psi[x])\frac{\sigma^2(x)}{2} \right\} p(x, t|x_0, t_0) \\ &= \int dx \psi[x] \left\{ -\partial_x[f(x)p(x, t|x_0, t_0)] + \partial_x^2 \left[\frac{\sigma^2(x)}{2} p(x, t|x_0, t_0) \right] \right\}. \end{aligned} \quad (33)$$

In the last line we have performed integration by parts, twice for the last term. Surface terms vanish by assuming $p(\pm\infty, t|x_0, t_0) = \partial_x p(\pm\infty, t|x_0, t_0) = 0$. By comparing (32) and (34) and noting that $\psi[x]$ is arbitrary we arrive at,

$$\partial_t p(x, t|x_0, t_0) = -\partial_x[f(x)p(x, t|x_0, t_0)] + \partial_x^2 \left[\frac{\sigma^2(x)}{2} p(x, t|x_0, t_0) \right]. \quad (34)$$

This is the Fokker-Planck equation for the conditional probability.

The potential and the stationary distribution

The Langevin equation (17) can be interpreted as the governing equation for a randomly forced massless classical viscous particle moving in a potential $U(x)$, where the drift term F is the negative derivative of the potential,

$$\dot{x} = -\frac{dU}{dx} + \sigma\eta. \quad (35)$$

The stable/unstable fix points for F corresponds to minima/maxima for U . The stationary distribution $p(x) \equiv p(x, \infty|x_0, t_0)$ will be independent of the initial state. For the process (35) the stationary distribution is obtained from solving the Fokker-Planck equation, observing that the stationary distribution is time independent, $\partial_t p(x) = 0$, and we have the ordinary differential equation,

$$d_x(pd_x U + \sigma^2 d_x p/2) = 0 \Rightarrow pd_x U + \sigma^2 d_x p/2 = c. \quad (36)$$

From the boundary condition $p(\pm\infty) = 0$ the integration constant must vanish, $c = 0$, and we have,

$$d_x U = -\frac{\sigma^2}{2} d_x \ln p \Rightarrow p = c_1 \exp(-2U/\sigma^2), \quad (37)$$

where the integration constant c_1 is determined from the requirement that $p(x)$ is a probability density, $\int p(x)dx = 1$. This important result states that the potential is simply minus the logarithm of the stationary probability density multiplied by half the the noise variance. For the special case of the harmonic potential $U(x) = \alpha(x - y)^2/2$, with equilibrium position at y , which is the Ornstein-Uhlenbeck process the solution to the time dependent Fokker-Planck equation (34) with initial condition $p(x, 0|x_0, 0) = \delta(x - x_0)$ gives,

$$p(x, t|x_0, 0) \sim \exp\left[-\frac{\alpha[x - y - x_0 \exp(-\alpha t)]^2}{\sigma^2[1 - \exp(-2\alpha t)]}\right]. \quad (38)$$

The evolution of the probability is now easy to understand. The maximum for the distribution is located at $y + x_0 \exp(-\alpha t)$, thus the system is drifting towards y with a 'speed' determined by the size of $-\alpha$, which is the drift term in (35). The variance at some small time t is $\sigma(t)^2 = \sigma^2[1 - \exp(-2\alpha t)]/2\alpha \approx \sigma^2 t$ which is characteristic for a diffusion process. Thus the last term in (34) is called the diffusion term.

The stationary distribution $t \rightarrow \infty$ gives a gaussian distribution function,

$$p(x) \sim \exp\left[-\frac{2\alpha (x - x_0)^2}{\sigma^2}\right], \quad (39)$$

from which we immediately obtain the fluctuation-dissipation theorem,

$$\langle (x - x_0)^2 \rangle = \frac{\sigma^2}{2\alpha}. \quad (40)$$

It is instructive to derive the fluctuation-dissipation theorem directly from the Langevin equation $dx = -\alpha x dt + \sigma dB$. The variance of the process is,

$$\begin{aligned} \langle (x + dx)^2 \rangle &= \langle (x - \alpha x dt + \sigma dB)^2 \rangle = \\ &= \langle x^2 \rangle + (\sigma^2 - 2\alpha \langle x^2 \rangle) dt + o(dt^2). \end{aligned} \quad (41)$$

Stationarity implies that the left hand side is identical to the first term on the right hand side and the fluctuation-dissipation theorem appears from the first order in dt terms.

The double well potential

Going beyond the linear regime more minima for U , separated by potential barriers, could exist. One example of such a situation is the Stommel two box ocean model. Taking the salinity to be the slow component, y , using that temperature adjusts much more quickly, and the freshwater forcing to be a white noise we end up with an equation of the form (35) where the potential U is a double well potential,

$$U(y) = 4\Delta \left(\frac{y^4}{4} - \frac{y^2}{2} \right). \quad (42)$$

Δ is the height of the potential barrier, shown in figure 6. Now, it is easy to imagine how this system will behave. If the variance of the noise is small in comparison to the potential barrier ($\sigma^2 \ll \Delta$) then the system will reside in one of the wells for a long time behaving essentially as in the case above. For ($\sigma^2 \gg \Delta$), on the other hand, the system will frequently jump from one minimum to the other. It can be shown, from the Fokker-Planck equation (34), that the typical waiting time τ can be expressed by the Arrhenius formula,

$$\tau \sim \exp(\Delta/\sigma^2). \quad (43)$$

The typical behavior of this system is shown in a numerical realization in figure 6 (b).

Stochastic resonance

We have a description similar to the one above in the Sellers-Bodyko types of energy balance models [17]. The two minima of the double well potential here corresponds to a glaciated and an ice-free planet. How can we now explain a periodic jumping from one state to the other? One way is to have a periodic changing of the potential such that the one stable state becomes unstable (through a saddle-node bifurcation), such that the system falls into the other state. Then by changing the potential back to the opposite situation where the new state becomes unstable and the system jumps back into the first state again. This is the usual hysteresis loop, shown in the cartoon in figure 8.

The problem with this description in connection with glacial cycles is that the periodically changing forcing from the variations in solar insolation (Milankovitch forcing) is too weak to be able to generate such a behavior. The Milankovitch forcing will rather result in a small wobbling as depicted in figure 8. If in this case the system also experienced a random forcing we would describe the system by (35) where the potential is defined by,

$$U(y) = 4\Delta\left(\frac{y^4}{4} - \frac{y^2}{2}\right) + U_1 y \cos(\omega t). \quad (44)$$

The potential barrier is now in the extreme case (for $t = 0$) asymmetric with a barrier height of $\Delta + U_1$ from one side and $\Delta - U_1$ from the other side. The time scales for penetrating the barrier from the shallow well (a) to the deep well (b) is then, $\tau_{a \rightarrow b} \sim \exp(-(\Delta - U_1)/\sigma^2)$, and the other way $\tau_{b \rightarrow a} \sim \exp(-(\Delta + U_1)/\sigma^2)$. If the system is to jump between the two climatic states periodically, with the period, $T = 2\pi/\omega$, we must have the variance, σ^2 , of the noise such that $\tau_{a \rightarrow b} \ll T$, else the potential barrier has grown before the system had a chance of penetrating the barrier. But on the other hand we must also have $T \ll \tau_{b \rightarrow a}$, else the system has time to jump forwards and backwards more times independently from the periodic changes of the potential. This means that there is a range for the variance of the noise in which the weak periodic forcing results in a noise induced periodic change in the climatic state. This is called a stochastic resonance [2, 29].

Ice-core records

Equipped with the basic tools for analyzing time series we will now examine one of the most important paleo-climatic records which exists. The ice-core records not only extend back in time into climate states different from the present, namely the last glacial period. They also have a high temporal resolution enabling an analysis of dynamics on a wide range of temporal scales. The ice-core to be analyzed here is obtained by coring at the summit of the Greenland ice-sheet. The ice-sheet is formed through snow deposition and can be viewed as an atmospheric sediment. The isotope ratio $^{18}\text{O}/^{16}\text{O}$ in the ice is a proxy for paleo-temperatures, while the dust concentrations in the ice yield information about the paleo-wind strength [23]. At the summit of the ice-sheet the ice-flow is slow and vertical thus an undisturbed $\delta^{18}\text{O}$ chronology for at least the last glacial cycle has been obtained through the deep ice-cores GRIP [10] and GISP2 [19]. The isotope ratio is defined as the deviation from the 'standard mean ocean water' (s.m.o.w.) and measured in permil; $\delta^{18}\text{O} \equiv \{[^{18}\text{O}/^{16}\text{O} - (^{18}\text{O}/^{16}\text{O})_{\text{s.m.o.w.}}]/(^{18}\text{O}/^{16}\text{O})_{\text{s.m.o.w.}}\} \times 1000$ permil. The ice-core record covering the past 90 kyrs is shown in figure 9 (a). The dating of the core, which is the translation of the depth to age, is done through counting of annual layers in the top of the record and using a flow model describing the thinning of the annual layers in depth where the annual cycle can no longer be resolved. The ice-core record of the last glacial cycle contained several surprises. Firstly, the present interglacial period seems to be very stable in comparison to the glacial period. Secondly, rapid climate changes between two quasi-stable states during the last glacial period were observed [9]. These shifts between interstadials, called Dansgaard-Oeschger (D-O) events, and stadials or deep glaciation have later been seen in Atlantic sediment records [4] and perhaps even in an isotope record from cave stalagmites in China being an East Asian Monsoon proxy [35]. This indicates a global extend of the D-O events. An essential part of estimating the anthropogenic climate changes is the evaluation of the natural variability of the climate itself. The ice-core records show indisputably very rapid and large climate changes in pre-historical times. Since the record is updated with very high temporal resolution and a precise dating, it is possible to extract information on various components of the climate system and to contrast different periods.

Separating time scales

The present climate is, in comparison to the climate of the last glacial maximum (LGM), relatively stable. The abrupt changes, D-O events, in temperature on time scales of a thousand years in the glacial period are associated with ice-surges, Heinrich events, from the large ice-sheets are not seen in the Holocene record. The presence of the ice-sheets impacts the atmospheric dynamics in glacial times. By comparison of very high temporal resolution ice-core records, covering the Holocene and the last glacial periods, we are able to observe differences in the coupled atmosphere-ocean dynamics between the two periods.

The ice-core data analyzed in the following, shown again in high resolution in figure 9 (a), covers the Holocene and the glacial period with a temporal resolution ranging from seasons in the present to approximately 10 years at 91 kyrs BP (17496 points). The data is based on sampling slices of specified increments down through the ice-core. The temporal resolution thus varies through the record due to the temperature dependence of the accumulation and thinning of the annual layers with depth. The mean resolution in the glacial period is 5.5 year averages with a maximum resolution of about 3.5 year averages near a D-O event. For details see reference [23].

The power density spectrum is calculated from interpolating the data series to regular time intervals. The spectrum is shown in Figure 10.

There are two regimes of behavior in the power spectrum separated at around a few hundred years. For time scales longer than 100 – 200 years the spectrum is a continuous red noise spectrum without dominant peaks signifying long time scale correlations. For time scales shorter than 100 – 200 years the spectrum is a white noise spectrum signifying short time scales or no temporal correlations. In order to separate the climate information of these two regimes we split the signal in the high and the low frequency part using a spectral cut at 150 years, figure 9 (b) is the 150 years low-pass, and (c) is the high-pass.

The characteristic "saw-tooth" D-O events are represented in the low-pass filtered signal. The climate dynamics of these events are related to surging and buildup of the ice-caps, and coupling to the ocean circulation. The surging is a very rapid process while the buildup takes more than a few hundred years, since the ice has to be transported as precipitation through the atmosphere. This could explain the saw-tooth shapes, which are maintained in the low-pass signal.

The residual high-pass signal, figure 9 (c), represents time scales faster than a few hundred years. This part of the signal contains the information on the atmospheric dynamics and the atmosphere-ocean couplings on the ENSO time scales of a few years. The most striking feature of this signal is that the envelope of the fluctuations is correlated with the degree of glaciation – or the temperature as represented by the $\delta^{18}O$ itself. Figure 9 (d) shows the 10 kyears low-pass of $\delta^{18}O$ (9 (a)) and figure 9 (e) shows the 10 kyears low-pass of the absolute value of the high-pass (9 (c)). The $\delta^{18}O$ signal is a proxy for the local temperature through the relation that in the cold climate, storm tracks move southward and the transport route for the precipitation is longer increasing the depletion of ^{18}O . Thus we interpret the increased variance as a direct result of a more stormy - or turbulent - state of the atmospheric flow during last glacial maximum (LGM).

Due to the presence of the ice-sheets and a substantially colder northern ocean in the glacial period larger thermal gradients between equator and the glaciers are expected than in the present climate. This would cause a more energetic and turbulent atmosphere through increased baroclinic activity in the glacial climate. This spectral analysis of the ice-core isotope record is the first observation of changes in the atmospheric circulation from paleoclimatic records for the LGM. It confirms atmospheric general circulation model (AGCM) studies of the LGM climate and indicates that the atmosphere was in a state characterized by more storminess and more variability.

The Dansgaard/Oeschger events

The changes in the state of thermohaline ocean circulation probably underlies the differences between the glacial state and the intermediate D-O state. Climate models of varying complexity from simple to fully coupled ocean-atmosphere general circulation models now more or less reliably reproduce the present and the glacial climate [34, 13]. However, at present the models are not capable of identifying the mechanisms responsible for the climatic changes observed in the records.

There are two major competing viewpoints for the occurrences of the shifts. The first viewpoint is that the shifts are caused by a de-stabilization of the state which the system occupies so that it is forced into the other stable state through a bifurcation [5, 28]. The second viewpoint is that internal fast time scale fluctuations acts as an effectively random forcing erratically triggering shift between quasi-stable climate states [8, 18, 6].

The first viewpoint is inspired by the demonstration [31, 37] that high resolution ocean models exhibits a bifurcation diagram similar to the one found in simple ocean box models [33]. In an 'intermediate complexity' climate model Ganopolski and Rahmstorf [15] recently simulated the D-O events by periodically forcing the model not quite to the bifurcation point, but such that the internal noise in the model induced a penetration of the reduced barrier. This is the stochastic resonance scenario [2].

The second viewpoint, that internal fluctuations in the system acts as a noise pushing the system across the barrier separating two quasi-stationary states, implies that de-stabilization of either state is irrelevant for the dynamics. From an analysis of the high resolution $\delta^{18}O$ climate proxy signal from the GRIP ice-core [23] it is possible to decide in favor of the latter of these two theories, namely that the shifts are governed by internal fluctuations. The way to decide between the two theories from data is by observing the distribution of waiting times between jumps from one state to the other. Here the waiting times are obtained as the times between consecutive separation points in the 100 years running mean of the isotope record. The separation points are identified as first up-crossings (down-crossing) through a constant level l_u (l_d) near the mean interstadial (stadial) level following a first down-crossing (up-crossing) through a constant level l_d (l_u) near the mean stadial (interstadial) level. This identifies the beginnings of the interstadial (stadial) states. The terminations are found by the same procedure run backwards in time. The times between termination of one state and beginning of the next is the transition time. This procedure identifies the D-O events in accordance with the visual identification performed by Dansgaard et al. [10].

Figure 11 (a) shows the distributions of durations of the glacial state in between interstadials and figure 11 (b) shows durations of the interstadials. Figure 11 (c) shows the pooled distribution. All three panels unambiguously show exponential distributions with mean waiting times of 1700 years, 1100 years and 1400 years respectively. The mean waiting times are represented by the slopes of the straight lines. The occurrence of exponential distributions indicates a Poisson process with noise induced transitions. This finding disfavors the proposals of periodic internal climate oscillations [20, 3, 30] or a stochastic resonance [1].

The climatic noise and intermittency

The high-pass signal in figure 9 (c) can be interpreted as a rough representation of the noise component inducing the climatic shifts. The noise is in this context variations on the time scales of the ENSO and other variations coupling the ocean and atmosphere. A characteristic of the state of the turbulent atmospheric flow is the intermittency or occurrence of extreme values in the temperature field as represented through the probability density function (PDF)[32]. In present day temperature records one finds gaussian PDF's when subtracting the annual and diurnal cycles. To compare this with the ice-core record, we can analyze the record covering the last 3 kyears. This part of the ice-core has been measured with a temporal resolution of approximately one month (26244 points). This is referred to as the Holocene (present climate) signal in the following. The Holocene signal is compared with the signal covering 14.4 – 29 kyears BP with a temporal resolution of approximately 3.7 years (3888 points), referred to as the LGM (Last Glacial Maximum) signal in the following. The Holocene signal has a white-noise power spectrum down to 5 – 10 years, see figure 10, where it bends of. This is similar to spectra obtained from present days climatological data [36]. Note the annual cycle in the spectrum. In order to subtract the low-frequency variability, related to non-atmospheric components of the climate system, we extract the high-pass filtered signal, and examine the PDF as a function of the high-pass cutoff frequency. The high-pass signal is normalized with the running variance in a window of 500 data points. The PDF's are fitted to Laplace type of distributions [24] of the form,

$$p_{\beta,\sigma}(x) = 1/(2^{1+1/\beta}\Gamma(1 + 1/\beta)\sigma) \exp(-|x/\sigma|^{\beta}/2), \quad (45)$$

which for $\beta = 2$ is the normal distribution and for $\beta = 1$ is the Laplace distribution. Figure 12 (a) shows the normalized 30 year high-pass for the Holocene signal, figure 12 (b) shows the cumulated distribution on a normal probability scale and figure 12(c) shows the fitted PDF. This signal is very close to being gaussian. Figure 12 (d),(e) and (f) shows the same for the normalized 30 year high-pass of the LGM signal. In this case there is a significant deviation from a gaussian distribution. The kurtosis, κ , and the best fit $\beta = \beta(\kappa)$ parameter, are shown in figure 13 as a function of the high-pass cutoff frequency. Triangles are Holocene – and diamonds LGM data. The error bars represent the 95 % confidence level [25]. The present Holocene climate shows a gaussian distribution for all time scales, while the

LGM signal becomes more intermittent for the faster time scales. This could indicate that the climate system was in a dynamical regime during the glacial period different from the present. From a naive point of view we would expect the glacial atmosphere to be in a state of more storminess during glacial times because the temperature gradient between the tropics and the ice-rim was much larger during the glacial times, where the polar regions were 20-30 degrees colder than today while the tropics were only about 5 degrees colder and the ice-rim of the glaciers was more advanced toward the tropics.

Exotic statistics

The observation of intermittency in the glacial record inspires to more speculative interpretations of the climatological time series.

In the following we will show that the Calcium record from the GRIP ice-core is consistent with the picture of a stochastic climate dynamics described by a Langevin equation and a bi-stable climate pseudo-potential is derived [12]. It is found that the fast time scale noise forcing the climate contains a component with an α -stable distribution. As a consequence of this interpretation the abrupt climatic changes observed could be triggered by single extreme events. These events are related to ocean-atmosphere dynamics on annual or shorter time scales and could indicate a fundamental limitation in predictability of climate changes.

The Calcium signal from the GRIP ice-core is the highest temporal resolution continuous glacial climate record which exists [14]. The logarithm of the calcium signal is (negatively) correlated with the $\delta^{18}O$ temperature proxy with a correlation coefficient of 0.8 [38, 27], thus we use the logarithm of calcium, figure 14 (a), as a climate proxy since it is related to dust in the ice and therefore does not diffuse in the ice and firn as the $\delta^{18}O$ signal does. The temporal resolution of $\log(\text{Ca})$ is about annual from 11 kyr to 91 kyr B.P. (80,000 data-points). This is an order of magnitude higher than that of $\delta^{18}O$. The probability density function (PDF) of the signal, figure 15, shows a bi-modal distribution with peaks corresponding to the warm interstadials and the glacial states.

From the premise of the stochastic dynamics represented by the Langevin equation and the data we can now uniquely determine the climate pseudo-potential, $U(y)$, and the structure of the noise term.

The noise term (diffusion term) is to first order, neglecting the drift term, defined as the derivative of the signal estimated as $(y_{t+\Delta t} - y_t)/\Delta t$, shown in

figure 14 (b). This signal is stationary except for a slow trend through the record which is partly due to smoothing with depth in the ice-core so that the intensity of the noise is approximately independent of $\log(\text{Ca})$. Note the implication that the intensity of fluctuations in calcium concentration is proportional to the calcium signal itself ($dx/dt = x d \log x/dt$) and thus to the degree of glaciation [11].

The noise has a strongly non-gaussian distribution. Figure 16 (a) shows the probability density function for the noise, figure 16 (b) shows the cumulated probability in a scale on which a gaussian distribution is a straight line (probability paper scale). Finally, figure 16 (c) shows the two tails of the distribution on a log-log plot magnifying the behavior of the tails. This has in an intermediate range a power function scaling with a power of about 2.75 and an additional extreme tail. The signal can be described by a Langevin equation,

$$dy = -(dU/dy)dt + \sigma_1 dx + \sigma_2 dL. \quad (46)$$

The first noise component, $\sigma_1 dx$, is generated by an additional Langevin equation, $dx = -xdt + \sqrt{1+x^2}dB$, where x is an (unmeasured) independent variable and dB is a unit variance Brownian noise. The stationary distribution for x is a t-distribution which fits to the observed tail distribution for the noise on y . The second noise term is an α -stable noise with stability index $\alpha = 1.75$. The α -stable distributions, corresponding to $\alpha < 2$, have cumulative probability tails which scales as $x^{-\alpha}$ implying that only moments of order less than α exists ($\langle |x|^\beta \rangle = \infty$ for $\beta \geq \alpha$). The α -stable distributions fulfill a generalized version of the central limit theorem, namely that the distributions of sums of identically distributed random variables with cumulative distribution tails scaling as $x^{-\alpha_1}$ converges to an α -stable distribution with $\alpha = \alpha_1$.

A generalization of the Fokker-Planck equation for the two coupled Langevin equations with α -stable noise excitations connects the stationary density solution to the pseudo-potential $U(y)$. However, only the marginal distributions are known since x is not observed. For y this is the PDF for $\log(\text{Ca})$ shown in figure 15. The pseudo-potential, shown in figure 17, is thus determined iteratively by simulation starting from a solution to the stationary one-dimensional Fokker-Planck equation using the marginal distribution.

In order to validate that the $\log(\text{Ca})$ signal can be described by (46), a simulation using the derived pseudo-potential, fitting σ_1 and σ_2 from the

noise structure of the signal, figure 16, should be compared with the $\log(\text{Ca})$ signal. The simulated signal is shown in figure 18, which should be compared with figure 14 (a). The thin lines in figures 15 and 16 are derived from the simulated signal. As seen in the figures the agreement between the data and the simulation is astonishing. Judged from different simulated realizations the two signals only deviate within the statistical uncertainty.

For the calcium data to be consistent with the dynamics described through a Langevin equation, the driving noise must be of the form described here. In order to understand the underlying climate dynamics it is important to establish the connection between this climatic proxy and the climate. It is especially important to interpret the two noise terms and connect them to the atmosphere-ocean dynamics. The presence of an α -stable noise component could imply that the triggering mechanisms for climatic changes are single extreme events. Such events, being on the time scale of seasons, are fundamentally unpredictable and never captured in present days numerical circulation models. All coupled general circulation models will due to smoothing and coarse resolution almost certainly show gaussian statistics. This could explain why these models have yet never succeeded in simulating shifts between climatic states.

Summary and outlook

Climate history recorded in ice-cores shows changes on many different time scales. By applying the time series analysis tools we obtain information about the dynamics of climatic changes. The glacial climate is much more variable than the present Holocene climate. On the time scales of a few years, where the most prominent climate variation in the present climate is the ENSO, we observe a more intermittently varying glacial climate. On time scales of hundreds to thousands of years the climate jumps between two quasi-stable states, the D-O state and the deep glacial state. The waitingtime distribution indicates a noise induced jumping. The stronger and more intermittent fast time scales variations in the glacial period could be the trigger. The weakening of this climatic noise could then be the reason for the apparent strong stability of the present Holocene climate. The cause for the more intense noise in the glacial climate could be a stronger temperature gradient between the tropics and the polar regions. The common paradigm is that the different quasi-stable states are caused by the existence of different

quasi-stable modes of the Atlantic thermohaline circulation [5]. However, the indications of D-O events in tropical paleoclimatic records challenge this view. Perhaps the ENSO, which is a strong tropical climate variation, plays an important role in the glacial climate variability [7]. Answering the question of the mechanism behind the observed natural climate changes is a future challenge and perhaps a benchmark for understanding the nature of present days antropogenic climate changes.

References

- [1] Alley, R.B., Anandakrishnan, S., Jung P., 'Stochastic resonance in the North Atlantic', *Paleoceanography*, 16, 190-198, 2001.
- [2] Benzi, R., Parisi, G., Sutera, A., Vulpiani, A., 'Stochastic resonance in climate change', *Tellus*, 34, 10-16, 1982.
- [3] Birchfield, E. G., Wang, H. and Rich, J. J., 'Century/millennium internal climate oscillations in an ocean-atmosphere-continental ice sheet model.
- [4] Bond G. et al., 'Correlations between climate records from North Atlantic sediments and Greenland ice', *Nature* 365, 143, 1993.
- [5] Broecker, W. S., 'Thermohaline Circulation, the Achilles Heel of Our Climate System: Will Man-Made CO₂ Upset the Current Balance?', *Science*, 278, 1582-1588, 1997.
- [6] Bryan, F., 'High-latitude salinity effects and interhemispheric thermohaline circulations', *Nature*, 323, 301-304, 1986.
- [7] Cane, M. A., 'Climate Change: A Role for the Tropical Pacific', *Science*, 282, 59-61, 1998.
- [8] Cessi, P., 'A Simple Box Model of Stochastically Forced Thermohaline Flow', 24, 1911-1920, 1994.
- [9] Dansgaard, W., Clausen, H. B., Gundestrup, N., Hammer, C. U., Johnsen, S. J., Kristinsdottir, P. M. and Reeh, N., 'A New Greenland Deep Ice Core', *Science*, 218, 1273-1277, 1982.
- [10] Dansgaard et al., 'Evidence for general instability of past climate from a 250-kyr ice-core record.', *Nature*, 364, 218-220, 1993.
- [11] Ditlevsen, P. D., Svensmark, H. and Johnsen, S., 'Contrasting atmospheric and climate dynamics of the last-glacial and Holocene periods', *Nature* 379, 810-812, 1996.
- [12] P. D. Ditlevsen, 'Observation of alpha-stable noise and a bistable climate potential in an ice-core record', *Geophys. Res. Lett* 26, 1441-1444, 1999.

- [13] Ganopolski, A., Rahmstorf, S., Petoukhov, V. and Claussen, M., 'Simulation of modern and glacial climate with a coupled global model of intermediate complexity', *Nature*, 391, 350-356, 1998.
- [14] Fuhrer, K., Neftel, A., Anklin, M., Maggi, V., 'Continuous measurements of hydrogen peroxide, formaldehyde, calcium and ammonium concentrations along the new GRIP ice core from Summit, Central Greenland', *Atmos. Environ., Part A*, 27, 1873-1880, 1993.
- [15] Ganopolski A. and Rahmstorf, S., 'Rapid changes of glacial climate simulated in a coupled climate model', *Nature* 409, 153, 2001.
- [16] Gardiner, C.W., 'Handbook of Stochastic Methods', Springer Verlag, N.Y., 1985.
- [17] Ghil M. and Childress S., 'Topics in Geophysical Fluid Dynamics: Atmospheric Dynamics, Dynamo Theory, and Climate Dynamics', Springer Verlag, N. Y. 1987.
- [18] Griffies, S. M., Tziperman, E., 'A Linear Thermohaline Oscillator Driven by Stochastic Atmospheric Forcing', *Journ. Climate*, 8, 2440-2453, 1995.
- [19] Grootes et al., 'Comparison of oxygen isotope records from the GISP2 and GRIP Greenland ice cores', *Nature*, 366, 552-554, 1993.
- [20] Grootes, P. M. and Stuiver, M., 'Oxygen 18/16 variability in Greenland snow and ice with 10^{-3} - to 10^5 -year time resolution', *Journ. Geophys. Res.*, 102, 26455-26470, 1997.
- [21] Hasselmann, K., 'Stochastic Climate Models', *Tellus* 28, 473-485, 1976.
- [22] Johnsen, S. J., Dansgaard, W. and White, et al., *Tellus* B41, 452-468, 1992.
- [23] Johnsen, S. J., et al., 'The $\delta^{18}O$ record along the Greenland Ice Core Project deep ice core and the problem of possible Eemian climate instability', *Journ. Geophys. Res.*, 102, 26397-26410, 1997.
- [24] Johnson, N. L. and Kotz, S., *Distributions in Statistics: Constant Univariate distributions II*, Wiley, N.Y., 1970.

- [25] Kendall, M. et. al., Kendall's Advanced Theory of Statistics, C. Griffin & CO. Lim., London, 1987.
- [26] Manabe, S. and Stouffer, R. J., 'Two Stable Equilibria of a Coupled Ocean-Atmosphere Model', Journ. of Climate, 1, 841-866, 1988.
- [27] Marsh, N. D. and Ditlevsen, P. D., 'Observation of atmospheric and climate dynamics from a high resolution ice core record of a passive tracer over the last glaciation', Journ. Geophys. Res., 102, 11219-11224, 1997.
- [28] Nakamura, M., Stone, P. H. and Marotzke, J., 'Destabilization of the Thermohaline Circulation by Atmospheric Eddy Transports', Journ. Climate, 7, 1870-1882, 1994.
- [29] Nicolis, C. 'Stochastic aspects of climatic transitions – response to periodic forcing', Tellus, 34, 1-9, 1982.
- [30] Paillard, D. and Labeyrie, L., 'Role of the thermohaline circulation in the abrupt warming after Heinrich events', Nature, 372, 162-164, 1994.
- [31] Rahmstorf, S., 'Bifurcations of the Atlantic thermohaline circulation in response to changes in the hydrological cycle', Nature 378, 145, 1995.
- [32] Sano, M., Wu, X. and Libchaber, A., 'Turbulence in helium-gas free-convection', Phys. Rev. A, 40, 6421-6430, 1989.
- [33] Stommel, H., 'Thermohaline convection with two stable regimes of flow', Tellus 13, 224-230, 1961.
- [34] Vettoretti, G., Peltier, W. R., McFarlane, N. A., 'Global water balance and atmospheric water vapour transport at last glacial maximum: climate simulations with the Canadian Climate Centre for Modelling and Analysis atmospheric general circulation model', Canadian Journ. Earth Sciences, 37, 695-723, 2000.
- [35] Wang, Y. J. et al., 'A High-Resolution Absolute-Dated Late Pleistocene Monsoon Record from Hulu Cave, China', Science, 294, 2345-2347, 2001.
- [36] Willebrand, J., J., 'Temporal and spatial scales of wind field over North-Pacific and North-Atlantic', Phys. Oceanogr., 8, 1080-1094, 1978.

- [37] Wright, D. G. and Stocker, T. F., 'A Zonally Averaged Ocean Model for the Thermohaline Circulation. Part I: Model Development and Flow Dynamics', *Journ. Phys. Oceanography*, 21, 1713-1724, 1991.
- [38] Yiou, P. et al., 'Paleoclimatic variability inferred from the spectral analysis of Greenland and Antarctic ice-core data', *Journ. Geophys. Res.*, 102, 26441-26454, 1997.

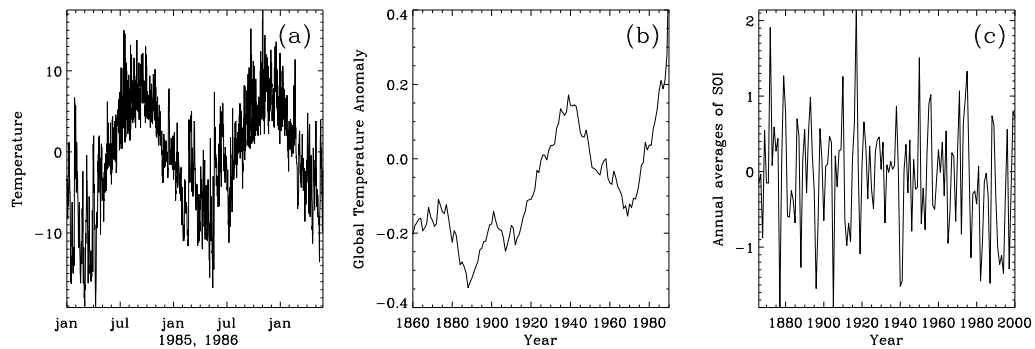


Figure 1: Three different climatic time series. (a) shows two years of the temperature record from the weather station in Nuuk, Greenland. The temperature is measured twice a day. (b) Shows the global temperature anomaly, defined as the global mean temperature subtracted the mean temperature for the period 1950-1979. The global mean temperature is obtained for the century long period where measurements have been done. The global mean is defined with a procedure for area averaging depending on the measurement coverage. The series is biased toward temperatures over land, since very few measurements exist over the oceans. The signal has been smoothed within a 10 years running window. (c) is the Southern Oscillation Index (SOI), which is defined as the pressure difference between a weather station in Tahiti and one in Darwin, Australia. The SOI is closely related to the El Nino in the Pacific ocean.

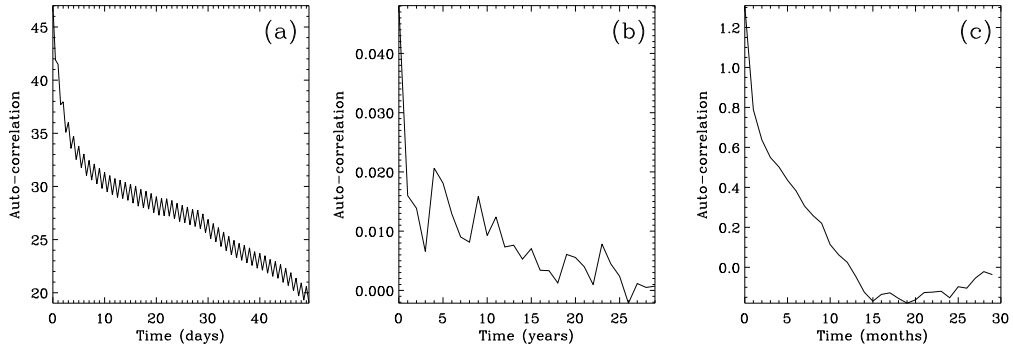


Figure 2: The auto-correlation functions corresponding to the three signals in figure 1. For the Nuuk temperature record (a) the auto-correlation is calculated from a 30 years record including the two years plotted in figure 1.

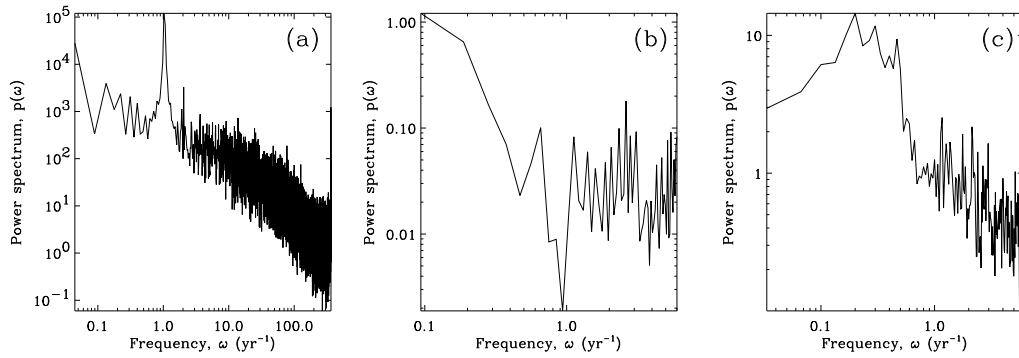


Figure 3: The power spectra for the three signals in figure 1.

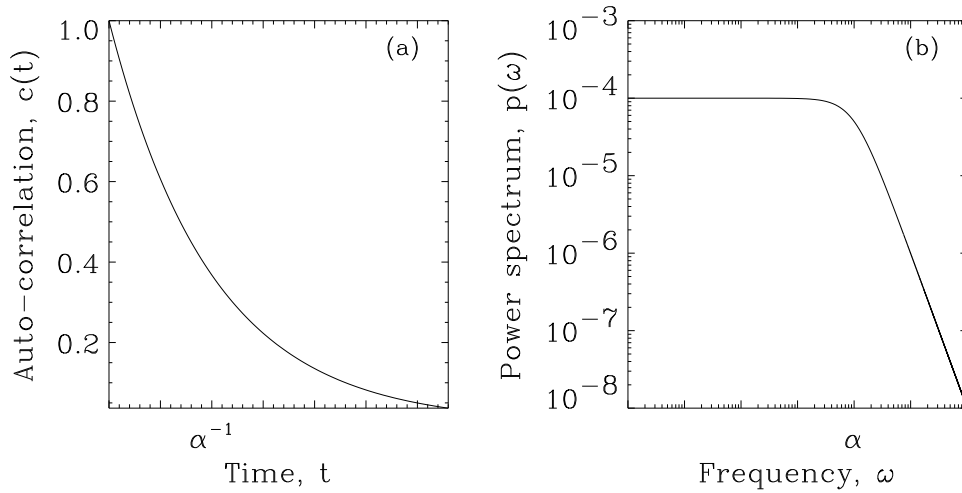


Figure 4: The auto-correlation function (a) and the power spectrum (b) for the climate variable y , governed by equation (18)

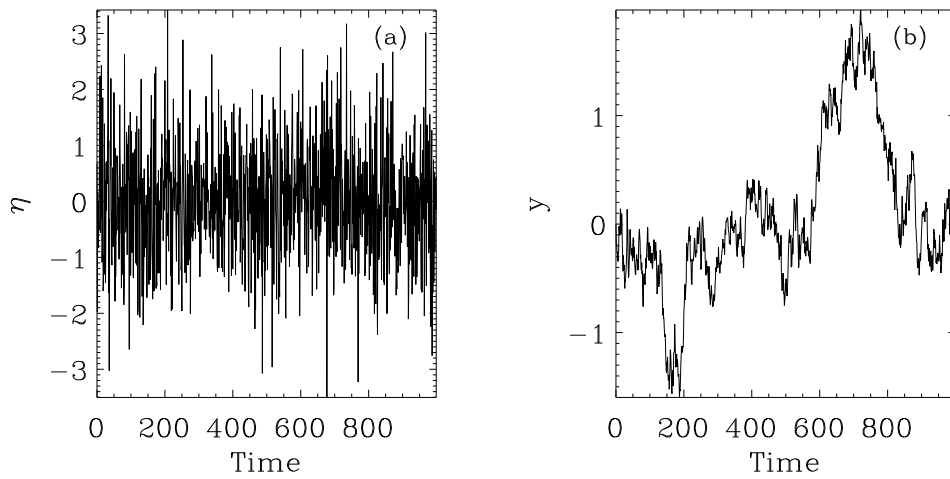


Figure 5: A simulation of the Langevin equation (18), (a) shows the white noise forcing, η . (b) shows the climate variable, y .

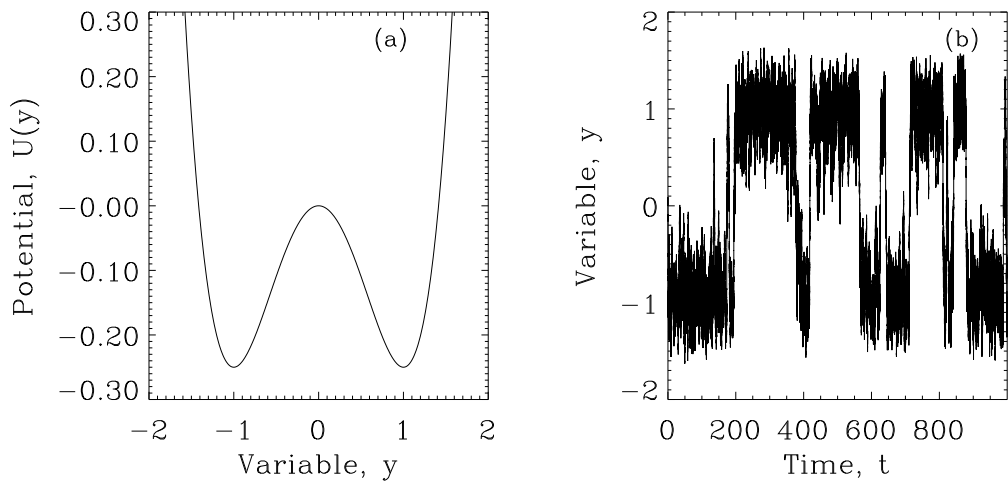


Figure 6: (a) A simulation of (35) with the double well potential shown in (b).

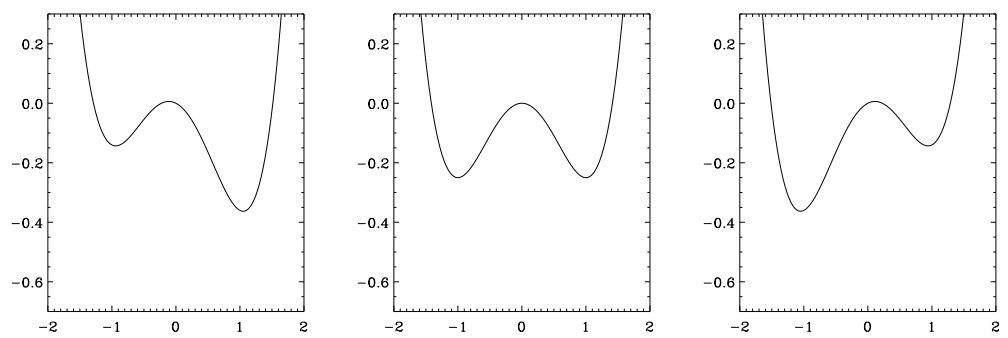


Figure 7: A weak periodic variation of the potential only changes the heights of the potential barrier.

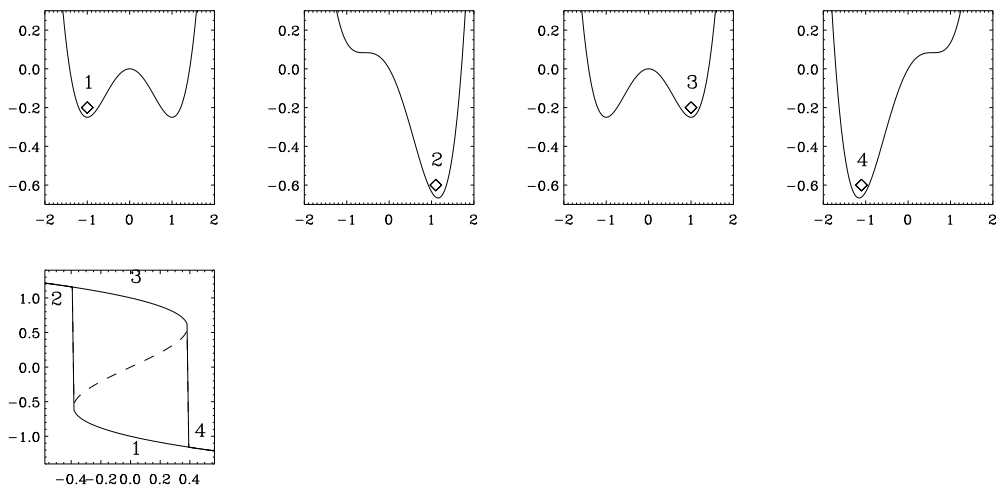


Figure 8: A strong periodic variation of the potential leads to hysteresis behavior through successive saddle-node bifurcations.

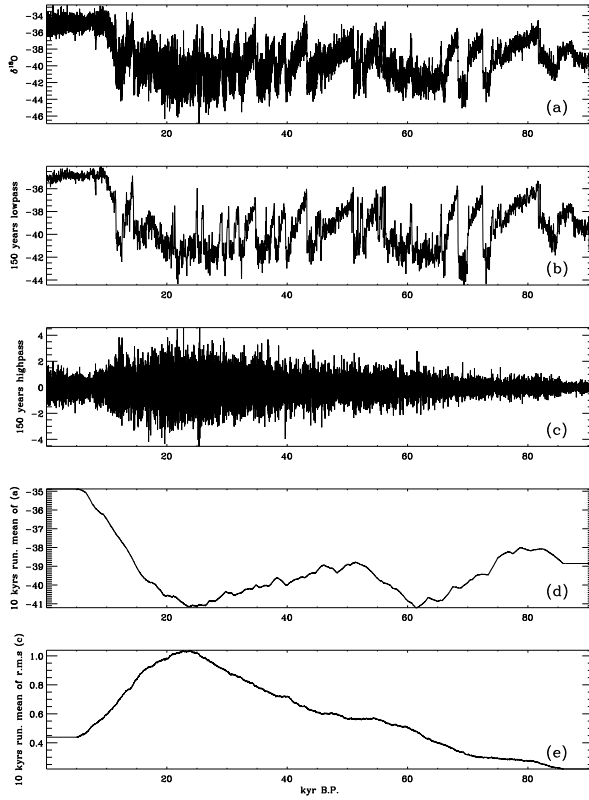


Figure 9: (a) The high resolution $\delta^{18}O$ signal from the Greenland ice-cap. $\delta^{18}O$ is the difference between ^{18}O content of the ice and ^{18}O content in present day's ocean water. Empirically it has been shown that there is approximately a constant linear relationship between $\delta^{18}O$ in precipitation and the air temperature where the precipitation falls [22]. The ice-cap thus constitutes a record, which is a proxy for the climate, as old as the ice itself that is of the order of 250 – 500 kyrs at the bottom. The exact relationship between temperature and isotope ratio depends in an intricate way on the sea/air temperature of evaporation, cloud temperature of condensation, and the path followed by the vapor before falling out as snowflake. Furthermore, the isotope ratio in the ice depends on molecular diffusion and mixing in the ice. The ice-core $\delta^{18}O$ ratio is therefore a proxy for some spatially and temporally averaged temperature signal, conditioned by a precipitation event. However, one can expect that these processes act as independent noise to the climatic temperature signal contained in the record. (b) is the 150 year lowpass of the $\delta^{18}O$ signal showing the D/O events, (c) is the corresponding residual 150 years highpass, which is just the difference between (a) and (b). (d) is the 10 kyres running mean of the $\delta^{18}O$ signal (a), and (e) is the 10 kyres running mean of the root mean square of (c).

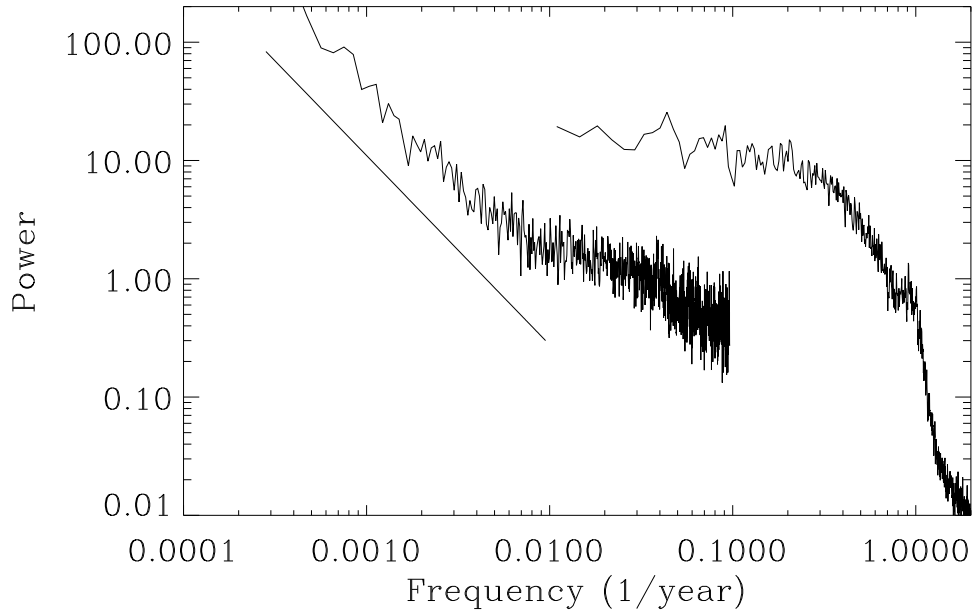


Figure 10: Power density spectra for the $\delta^{18}O$ record covering 0 – 91 kyear BP with a temporal resolution of approximately 10 years at 91 kyears BP (17496 points). The rightmost, Holocene, spectrum covers 0 – 3 kyears BP, with a temporal resolution of approximately 1 month (26244 points). The spectrum has a spectral slope of approximately -1.6 for time scales larger than 100 – 200 years, indicated by the sloping line. For time scales smaller than 100 – 200 years the spectrum is white until timescales of 5 – 10 years. The strong damping of the high frequencies corresponding to time scales smaller than 5 – 10 years is partly due to diffusion of the signal in the firn and ice. Note the annual peak in the spectrum.

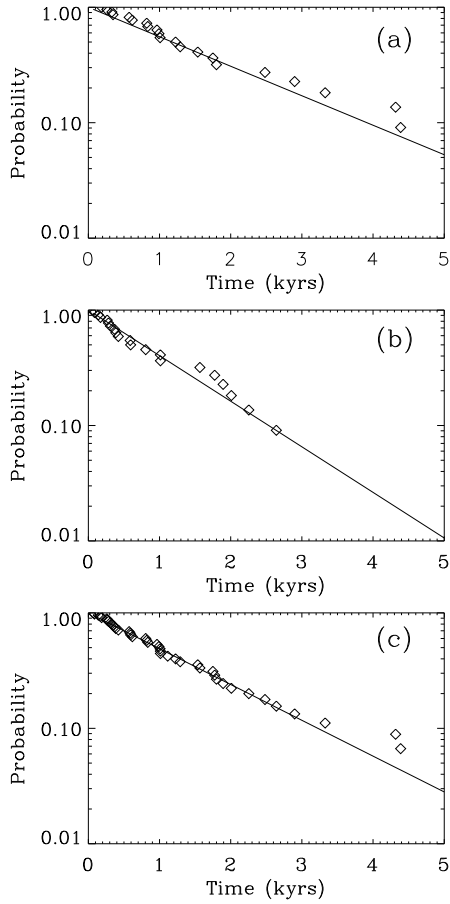


Figure 11: The distribution of waiting times between consecutive crossings of an upper and a lower level corresponding to the inter-stadials and stadials respectively. Probabilities $P(\tau > t)$ of a waiting time τ longer than t as a function of t are plotted. The straight lines represents exponential distributions. Panel (a) shows the waiting time from entering a stadial state to entering an interstadial state, the straight line is an exponential with mean waiting time of 1700 years. Panel (b) shows the same for waiting times from entering an interstadial until going to a stadial. The straight line is an exponential with mean waiting time of 1100 years. Panel (c) shows the distribution of the pooled waiting times from entering one state until entering the other state. The straight line is an exponential with mean waiting time of 1400 years.

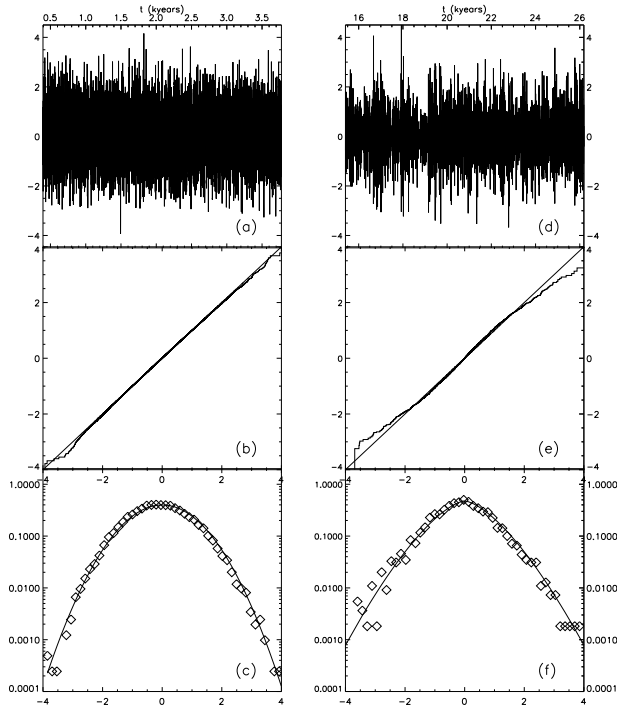


Figure 12: (a) The 30 years highpass filtered Holocene signal, covering 0 – 3 kyears BP (26244 points). The signal is normalized with the variance in a 500 points running window, (b) is the cumulated probability on a normal probability scale, (c) is the PDF, which is gaussian. The right panels (d),(e),(f) are the same as (a),(b),(c) but for the LGM signal, covering 14.4 – 29 kyears BP (3888 points). This signal is intermittent.

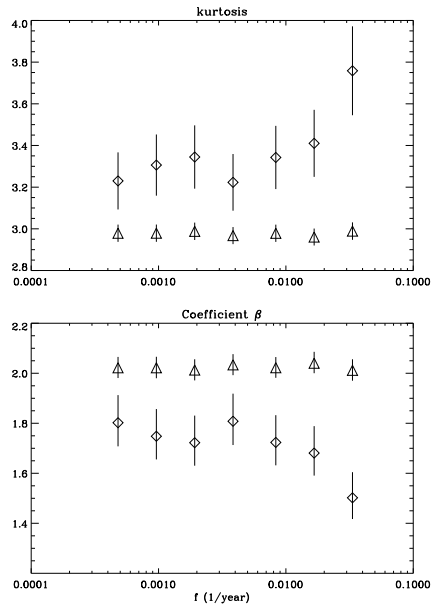


Figure 13: (a) The kurtosis, $\kappa \equiv \langle x^4 \rangle / \langle x^2 \rangle^2$, as a function of the highpass cutoff frequency. The kurtosis is 3 for the gaussian distribution and 6 for the laplacian distribution. Triangles are for the Holocene and diamonds for the LGM. The errorbars are the 95 % confidence levels. The Holocene signal is gaussian for all cutoffs, while the LGM becomes more intermittent when subtracting the longer timescales.

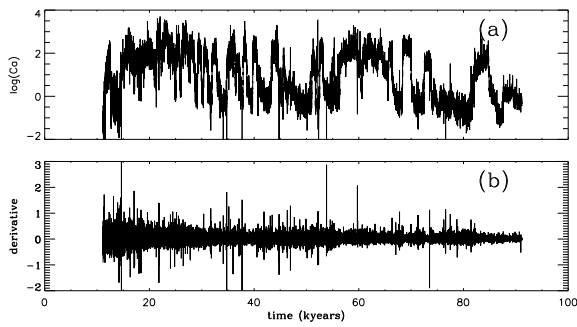


Figure 14: (a) The logarithm of the calcium concentration as a function of time (BP) in the GRIP ice-core. The dating of this upper part of the record is rather precise. The temporal resolution is about 1 year, much better than the $\delta^{18}O$ record since the dust does not diffuse in the ice. The signal is a proxy for the climatic state. (b) The derivative of the signal in (a). This approximately stationary signal is strongly intermittent.

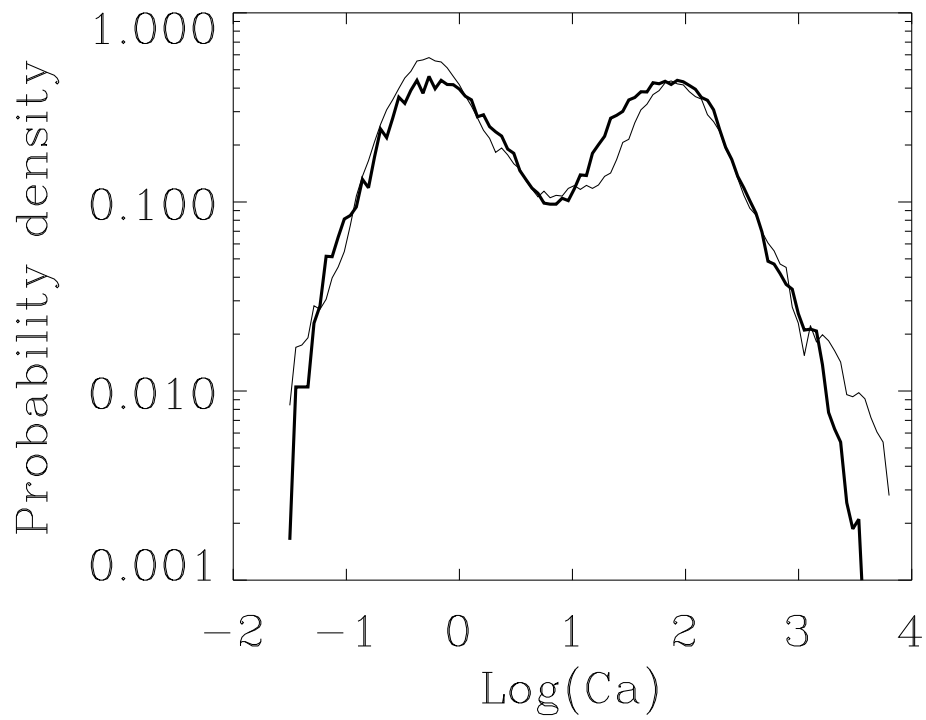


Figure 15: The probability density function (PDF) of the $\log(\text{Ca})$ signal shows the bimodal distribution. The thin curve is the PDF of the simulated signal (figure 18).

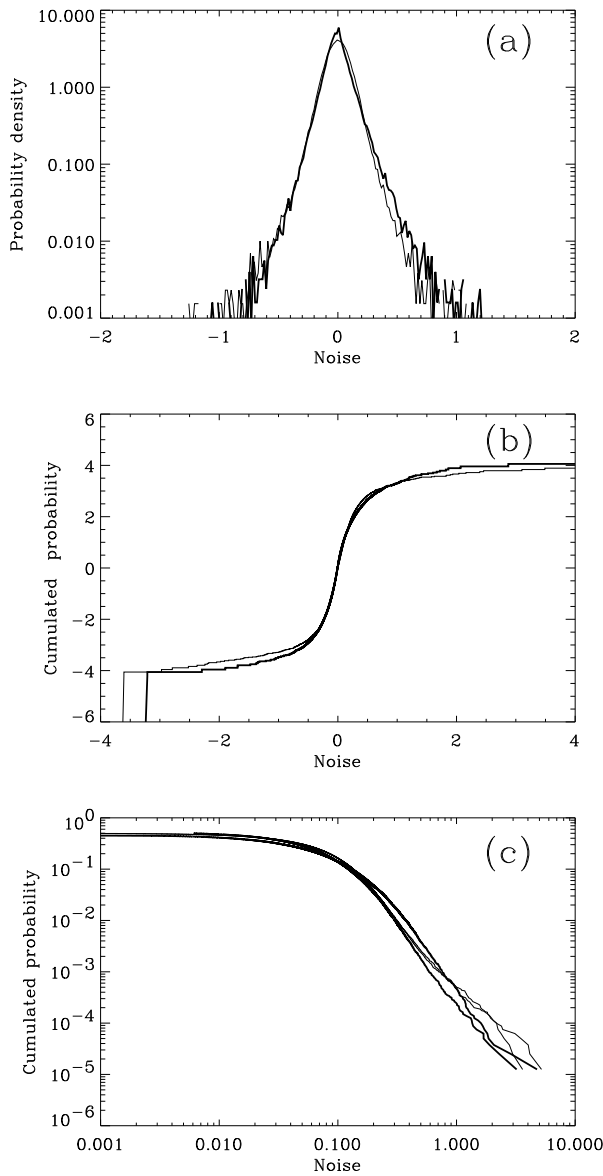


Figure 16: (a) The probability density of the noise (figure 14 b). (b) The cumulated distribution of the noise. The scale is a 'probability paper scale' where a gaussian distribution shows up as a straight line. This signal is strongly non-gaussian. (c) The two tails of (b) on a log-log plot. For the upper tail the probability of values larger than the abscissa is shown. The thin curves are from the simulation, showing that the signal is well described as containing a t-distributed noise component and an α -stable noise component.

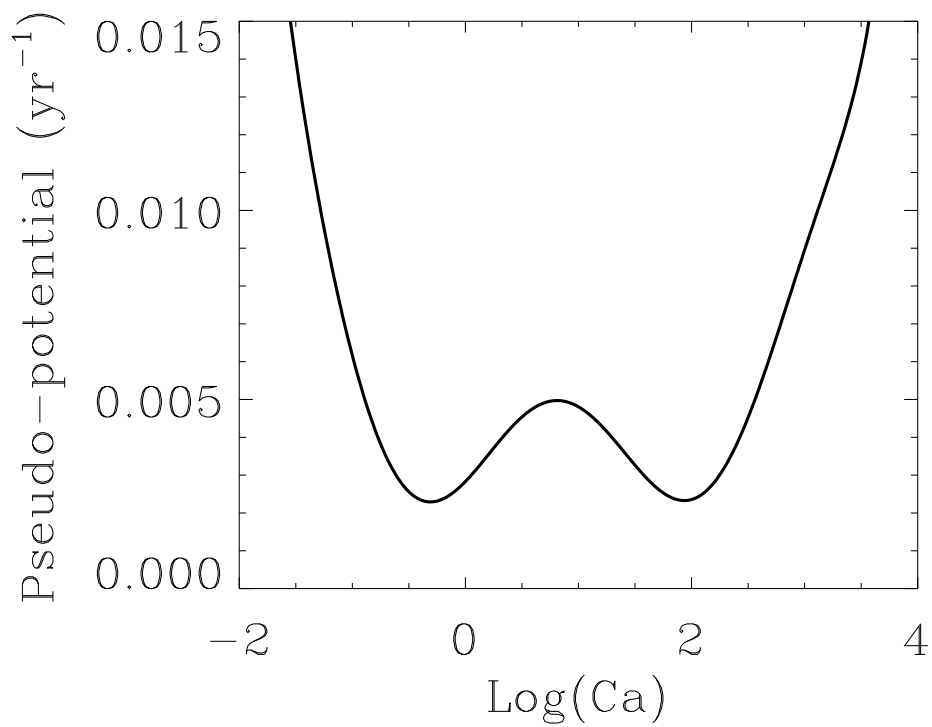


Figure 17: The climate pseudo-potential is a double-well potential with the left well representing the interstadial state and the right well representing the full glacial state. The potential is obtained from a generalized stationary Fokker-Planck equation.

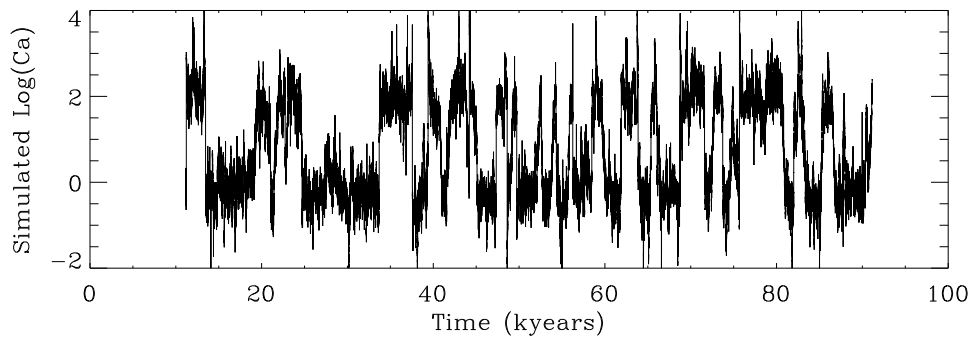


Figure 18: An artificial $\log(\text{Ca})$ obtained from simulating a sample solution to the Langevin equation using the climate pseudo-potential, an $\alpha = 1.75$ white noise and $\sigma_1/\sigma_2 = 3$. This should be compared to figure 14 a. The two signals are statistically similar, showing that the $\log(\text{Ca})$ signal can be generated by the stochastic dynamics.